Laterally Modulated Excitation Microscopy: Improvement of resolution by using a diffraction grating

R. Heintzmann*, C. Cremer

Applied Optics and Information Processing Division
Institute of Applied Physics,
University of Heidelberg
Albert Ueberle Str. 3-5
D-69120 Heidelberg

ABSTRACT

High spatial frequencies in the illuminating light of microscopes lead to a shift of the object spatial frequencies detectable through the objective lens. If a suitable procedure is found for evaluation of the measured data, a microscopic image with a higher resolution than under flat illumination can be obtained.

A simple method for generation of a laterally modulated illumination pattern is discussed here. A specially constructed diffraction grating was inserted in the illumination beam path at the conjugate object plane (position of the adjustable aperture) and projected through the objective into the object. Microscopic beads were imaged with this method and evaluated with an algorithm based on the structure of the Fourier space. The results indicate an improvement of resolution.

Keywords: Resolution Improvement, Lateral Modulation, Fringe Projection, Fluorescence Microscopy, Diffraction Grating

1. INTRODUCTION

Three dimensional fluorescent microscopy is an important tool in many fields of science. Many of its applications depend on a high resolution. In conventional epifluorescence microscopy, the resolution is limited by the aperture of the objective lens ($NA_{ObjLens}$). When imaging an incoherent light source as in fluorescence microscopy, the resolution can be defined as the radius of the first minimum of the Airy disc when imaging a point-source (Rayleigh criterion) :

$$r_{Airy} = 0.61\frac{\lambda_0}{NA_{ObjLens}}$$

, where λ_0 is the wavelength of the emitted light in vacuum. $NA_{ObjLens}$ is the product of the sine of the half-angle (α) of the cone of light entering into the objective lens and n the diffraction index of the immersion medium. For an emission wavelength of 530 nm (emission of fluoresceinisothiocyanate, FITC) this results into a minimum object distance of about 230 nm to be resolved for $NA_{ObjLens} = 1.4$. For the full width at half maximum (FWHM) of the point spread function (PSF) the factor 0.61 is replaced by 0.52 resulting into approximately 200 nm FWHM of the PSF for the example above mentioned. Under practical circumstances usually valid in biological application, this resolution is difficult to achieve due to an imperfect beampath.[1]

2. LATERAL MODULATION

If a lateral modulation is applied to the illuminating light, the range of measurable spatial frequencies is expanded. The lateral modulation can be described in the simplest case by a sinusoidal modulated excitation intensity structure with modulation depth m

* Email: rheintz@popeye.aphys2.uni-heidelberg.de

$$I_{ex}(x,y) = I_0\,(1 + m\cos(\Delta k_x x + \Delta k_y y + \varphi_0)) \quad (1)$$

$$= I_0\left(1 + m\frac{e^{i(\Delta k_x x + \Delta k_y y + \varphi_0)} + e^{-i(\Delta k_x x + \Delta k_y y + \varphi_0)}}{2}\right) \quad (2)$$

$$= I_0 \cdot FT\left(\delta\left(\vec{k}\right) + \frac{m}{2}e^{i\varphi_0}\cdot\delta\left(\vec{k} - \vec{\Delta k}\right) + \frac{m}{2}e^{-i\varphi_0}\cdot\delta\left(\vec{k} + \vec{\Delta k}\right)\right) \quad (3)$$

, where I_0 is the mean intensity in the object plane, Δk_x and Δk_y are the respective components of the modulation k-vector $\vec{\Delta k}$ as shown in Figure 1B). A function depending on $\vec{k}$ indicates, that it is a function in Fourier space (reciprocal space, k-space). A function in real space depends on of the cartesian coordinates $\vec{r}$ or of its individual components x, y or z (x, y lateral, z axial). We assume the emission intensity $I_{em}(\vec{r})$ to depend linearly on the excitation intensity $I_{ex}(\vec{r})$ and the concentration of fluorescent substance $Obj(\vec{r})$. Thus with a suitably normalised $Obj(\vec{r})$, $I_{em}(\vec{r})$ can be written as $I_{em}(\vec{r}) = Obj(\vec{r})\ I_{ex}(\vec{r})$. Applying the Fourier convolution theorem results for the Fourier transform (FT) into:

$$FT(I_{em}(\vec{r})) = FT(Obj(\vec{r})) \otimes FT(I_{ex}(\vec{r}))$$

Since $FT(I_{ex}(\vec{r}))$ consists of three distinct peaks in Fourier space, the object structure is present in three shifted copies in the emission intensity structure. Their relative phases depend on the phase of the excitation intensity φ_0.

The incoherent imaging process of an epifluorescence microscope results in a convolution of its point spread function $PSF(\vec{r})$ with the emission intensity distribution $I_{em}(\vec{r})$. Thus the detected intensity $I_{det}(\vec{r})$ can be written as a multiplication of the emission intensity with the optical transfer function $OTF\left(\vec{k}\right) = FT(PSF(\vec{r}))$ in Fourier space : $FT(I_{det}(\vec{r})) = FT(I_{em}(\vec{r}))\cdot OTF\left(\vec{k}\right)$. The $OTF\left(\vec{k}\right)$ has a finite region in Fourier space that is not equal to zero called its region of support (see Figure 1A). The region of support defines the resolution of the system. If each copy of the object Fourier space structure can be extracted and shifted to the origin, the range of overall detectable frequencies can be substantially extended as shown in Figure 1. The region shown in C is given by the correlation of A with B.

The range of C depends on the spatial frequencies contained in the illumination pattern. The maximum lateral spatial frequency detectable is given by Δk_{max} in Figure 1C. With a spatially modulated illumination pattern being transmitted through the objective lens an enlargement of the lateral size of the region of support of the OTF up to a factor of two can be achieved. The factor of two is obtained if $\Delta k_{Imax} = \Delta k_{Lens}$ (see Figure 1).

Note (Figure 1C), that there can be also an axial resolution improvement for most lateral frequencies ($k_{x,y}$) in the object (especially very low and very high frequencies). As noted by T. Wilson et al.,[2] this method can be used to improve the axial resolution of the microscope and make optical sectioning in a standard non-confocal microscope possible. This is especially interesting since a standard epifluorescence microscope can not discriminate a lateral plane ($k_x = 0$) in the axial direction. This method is therefore also used in the examination of the 3D structure of surfaces called topometry with the "fringe projection technique", described by Windecker et al..[3] The region of support of the 3D-OTF extends almost as far as in a confocal microscope. In the case of illumination with an incoherent light source, there is a decoherence effect, that fades the modulation at an axial distance from the focus point and may increase the axial resolution additionally. In contrast to confocal microscopy, there can be a relatively high energy content in high frequencies in the illumination pattern. This increases the signal to noise ratio for high object frequencies. The detection efficiency for the shifted object structures has its maximum at an object frequency of Δk_{Imax} in Figure 1B,C.

The whole process of illumination, microscopic imaging and image reconstruction (see below) was simulated with pointlike objects resulting into an overall PSF under ideal conditions (Figure 1 Right). In the simulation for an emission vacuum wavelength of 530 nm, $\Delta k_{Imax} = \Delta k_{Lens}$ and $NA_{Objective} = 1.4$ a FWHM of the PSF of 188 nm was obtained for conventional microscopy and a FWHM of 95 nm for the method of laterally modulated excitation microscopy (LMEM) in combination with the algorithm described below.

A straightforward way to obtain a spatially modulated excitation pattern is to put a diffraction grating in the illumination beam path, at in the conjugate object plane where usually the adjustable aperture is situated (see Figure

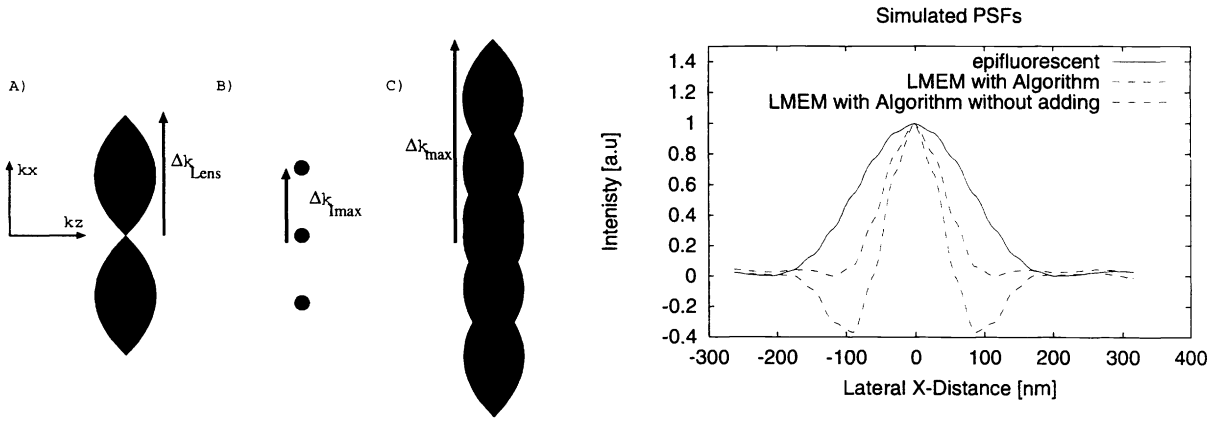

Figure 1. *Left: A):* Region of support (where the OTF is not equal to zero) of a normal epifluorescence OTF. This region is rotationally symmetric with respect to the optical axis (about k_z). *B):* Structure of the incident Light OTF when projecting a grating described by formula 2. *C):* Region of support of the total intensity OTF of the system which is the correlation of A and B. *Right:* Simulated PSF for a normal epifluorescence microscope and PSF using lateral modulated excitation microscopy (LMEM). The calculation was done for 530 nm emission vacuum wavelength, NA=1.4 and $\Delta k_{Imax} = \Delta k_{Lens}$. Note that values in the PSF below zero can appear, when the reconstruction step 6 in the algorithm described below is omitted.

2). The diffraction grating is then scaled down onto the object by the objective lens (as used by Wilson et al.[2]). Illuminating this grating in a normal epifluorescence microscope yields a simple spatially modulated illumination intensity. When only the zeroth and the ± first order of the diffraction grating pass the objective lens, this will result in a sinusoidal illumination intensity, whose modulation depth in focus depends on the quality of the grating, and on the optical transfer function of the objective (the transmission efficiency for the high spatial frequencies of the grating). The limitation to the grating spacing, that can be projected is given by the resolution of the objective. The numerical aperture of the objective must allow to transmit at least the plus and minus first diffraction order of the grating.

3. EXPERIMENTAL SETUP AND METHOD

A Zeiss (Standard 25) epifluorescence microscope was used in the experimental observations. It was equipped with a motorised XYZ table for object positioning (1 Step=10 nm). Excitation of the fluorophores was performed by illuminating with a Hg-Vapour light source filtered by an appropriate beam splitter cube. Images were taken using a CCD-Camera (Kappa CF8-RCC) equipped with a 2x image expander for sufficient pixel sampling rate. An objective lens (PL FLUOTAR 63x, NA=1.4 Oil) was used for the detection as well as for the illumination beampath.

The microscope was modified in the illumination beampath (see Fig. 2). A diffraction grating was specially constructed for this purpose by photo-lithographic techniques consisting of rectangular shaped aluminium coated bars on a glass support (grating distance $d = 30\,\mu m$, 50% Al-coated area) and inserted into the illumination beampath in front of the light source. It replaced the adjustable illumination aperture. This grating was adjustable into the axial direction for fine tuning of its position. The exact alignment was then performed by observing and manually maximising the modulation of the projected pattern onto the focused beads by manually moving the grating along the optical axis while projecting the grating into the object.

Microscopic beads 140 nm in diameter, stained with FITC, and quartz beads[4] 416 nm in diameter stained with Rhodamine Isothiocyanate (RITC) in the 200 nm core) were imaged using the method of lateral modulated excitation microscopy. The motorised table allowed the movement of the object relative to the projected grating fringes. In the experiment, a number of images where measured moving the X-Stepping motor between them by 40 nm. From these data, four images having a phase shift of the illumination grating relative to each other of approximately 90° were taken. These images are referred to as 0° (reference image) 90°, 180° and 270° image. After having taken these

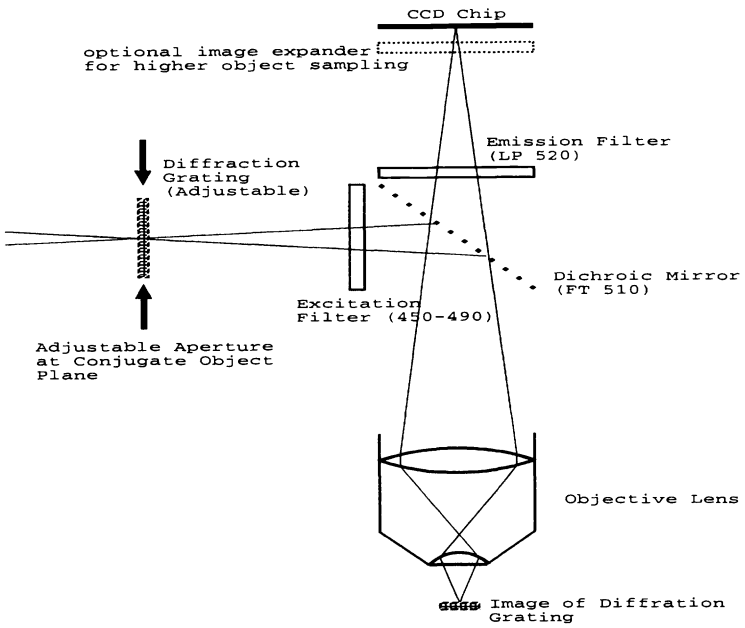

Figure 2. The illumination beampath of an epifluorescence microscope was modified by inserting a diffraction grating at the conjugate object plane (position of the adjustable aperture). It was imaged into the object by the objective lens system (63x, NA=1.4 Oil). The grating constant was 30 μm (resulting in 476 nm fringe distance in the object). For sufficient sampling an image expander (2x) was inserted before the CCD camera.

images, the grating itself was turned by hand by approximately 90 degrees so that the grating vector pointed into a direction perpendicular to the first. With the same method a second set of images was then obtained from the same object region.

4. ALGORITHM FOR DATA EVALUATION AND RESULTS

The difficulty that arises in evaluation of the data is to separate the components of different illumination frequencies from the measured data and shift them back to the central position with the correct phase in the Fourier space for reconstruction of the image. In principle, the data could be reconstructed from three linearly independent images by solving the associated equation system for the images. However, four images with phase differences make the reconstruction more straightforward. This method was therefore used. The phase structure of the object frequencies can be seen in Figure 3 and be followed through in Figure 4. The reconstruction of experimental data (beads with 140 nm diameter) and its Fourier transforms can be seen in Figures 5 to 7.

At first, the images taken under one angle of the diffraction grating were processed. Images taken under the perpendicular angle were processed afterwards and then added to the result of the first.

The evaluation of the measured data (LMEM reconstruction algorithm) consisted of "preparation" and "reconstruction" steps.

Data Preparation

1. The first image taken, was defined as the object reference image.
2. All other images were shifted, so that their object positions aligned with the positions in the reference image. This was done by using a Fourier space based algorithm. Evaluation of the centre of mass of the maximum (and 2 more pixels in each dimension, clipped at the minimum of this region) of the cross-corelation of the image

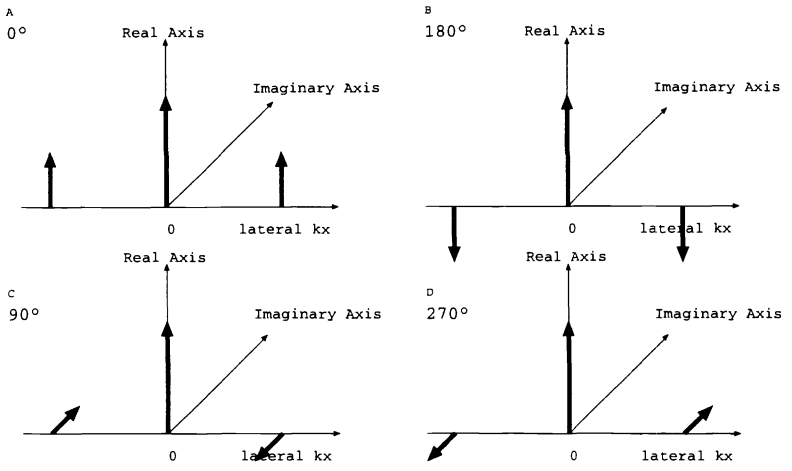

Figure 3. Different phases of the illumination light in laterally modulated excitation microscopy. A global phase of the reference image (0°) can be thought as rotation of the left arrows clockwise and the right arrows counterclockwise.

with the reference image yielded a shift-vector ($\vec{x}$) with subpixel accuracy. This method worked accurately, because the images were dominated by the zero diffraction order of the grating. The image was shifted by multiplying the Fourier transform of the image with $exp(i\vec{k}\vec{x})$ and transforming it back to real space (not shown in the figures).

3. A different scaling (due to photobleaching) and a different offset was compensated automatically. At first the high frequency energy content was computed by summing the absolute square of spatial frequencies greater than 10% of the maximum frequency in the Fourier space for the reference image and the image to be corrected. Then the bleaching ratio was determined by computing the squareroot of the ratio of these energies. Afterwards the offset of the image was corrected by adjusting its zero frequency value (the mean value in the real space image) to match the value of the reference image.

The sinusoidal illumination light (see formula 2) results in three points in Fourier space (the three arrows in Figure 3A that are drawn, without restricting the generality, into direction the real axis). These are convoluted in Fourier space with the Fourier transform of the object (not shown in Figure 3). The emission structure has to be multiplied in Fourier space by the detection OTF that has its maximum in the centre ($k_x = 0$) and decays down to the cutoff frequency (k_{max}) as indicated in Figure 4D. During the reconstruction process the individual components of the object structure in Fourier space were extracted and shifted with the correct phase to the position where they would belong at a flat illumination. A view of an experimental image of 140 nm beads after the preparation steps is shown in Figure 5(a,b). The strong zero frequency peak in Fourier space (central peak) from illumination with the zero diffraction order can clearly be seen. The two small side peaks are so weak, that they can hardly be distinguished in this image. At first (as in Figure 5) the grating had its modulation vector into the vertical direction.

Data Reconstruction

1. The 180° image was subtracted from the 0° image. In the Fourier domain the zero order was therefore eliminated (Figure 4A). Figure 5(b) shows the modulation from the modulated excitation on the clustered beads. This can also be seen as the two sidepeaks in Figure 5(d). Some artifacts of the CCD-camera and the high frequency noise was removed by removing the high frequencies in the Fourier domain.

2. The 270° was then subtracted from the 90° image (Figure 4B). This yielded a 90° phase-shifted result. Note the different phase compared to above, especially on the single beads in the image 5(e).

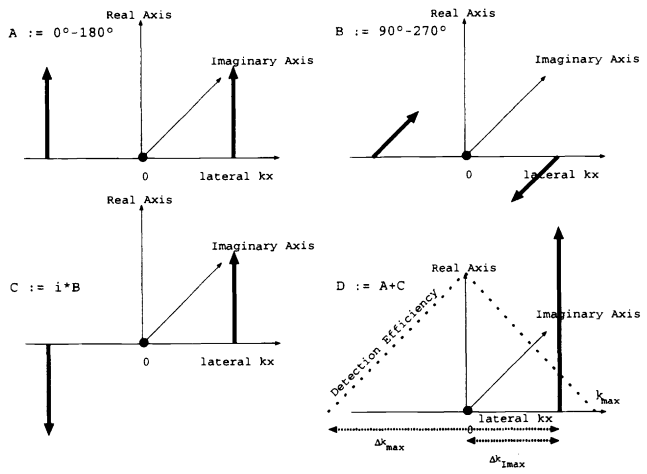

Figure 4. The figures (A to D) show the phase structure in different steps during the reconstruction process. The individual illumination phases are shown in Fig. 3. The object structure is also processed and does cancel in exactly the same way as the illumination arrays do. A global phase of the reference image (0° in Figure 3) only influences the resulting phase in D.

3. The result of step 2 was multiplied by the complex constant i (Figure 4C) and subtracted from the result of step 1 (Figure 4D). This resulted in only one remaining peak in the Fourier space together with its associated object structure in the Fourier space multiplied by the OTF of the microscope. Figure 6(a,b) shows the result of this step. The only remaining peak of the zero object frequency can now be seen in Figure 6(b).

4. The image was shifted in Fourier space by multiplying the real-space image with $exp(i\vec{k}\vec{x} + \phi_0)$, where the $\vec{k}$ depends on the grating constant and direction. The global phase ϕ_0 was automatically determined so that the zero-frequency peak (= the complex mean of the image) of the shifted image was real and positive. It depends on the initial phase of the illumination of the reference image (0°). As can be seen in Figure 6(d) the zero object frequency was shifted back into the zero-frequency position.

5. The complex conjugate of this image was added to itself in real-space. The result of this was a real valued image that had an improved resolution in one lateral direction (Figures 6(e,f)). However, the suppression of the low frequencies yielded negative values in the image and a overestimation of the edgelike structures. As can be seen in Figures 6(c) and (e), the real component of the image remains the same.
   Images taken with a grating rotated by 90 degrees, thus having a perpendicular direction of diffraction and grating vector were processed up to this step (Figures 7(a,b)). Now that the modulation was performed into the horizontal direction, this resulted into an enlargement in Fourier space perpendicular to the image above. This result was then added to the other image (Figures 7(c,d)).

6. The mean of all images 0°, 90°, 180° and 270° was added with an empirically determined weight after processing them up to the preparation step 3 to the result of reconstruction step 5. The same weight of 1/26 was used for all experimental data shown and chosen such, that only very small negative values occur in the image.
   This restores the low frequencies without disturbing the high frequencies, since the high frequencies of opposed images (like 0°and 180°) cancel each other (see from Figure 3). Therefore only a "normal" microscopical image (flat illumination) remained (see Figure8 left side). This was weighted and added to the result of step 5.

All reconstruction steps 1 to 6 can be carried out with a computational effort of O(N) on the real-space images (N being the number of Pixels in the image). Preparation step 2 is not necessary, if the grating is shifted instead of the object and a sufficiently high sampling is used. Preparation step 3 is not necessary if the approximate amount of photobleaching is known in advance. Therefore the overall performance of this algorithm could be O(N) and sufficiently fast for online processing.

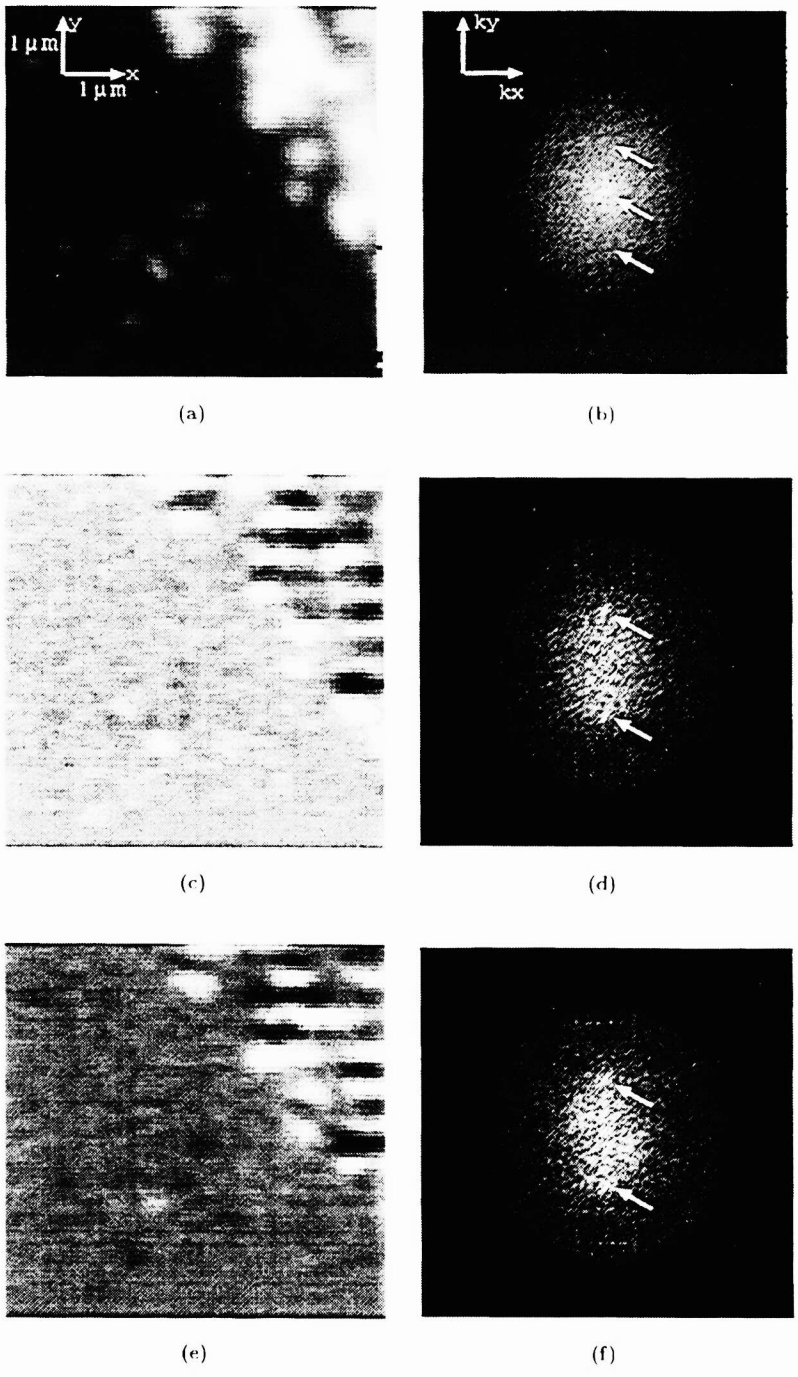

Figure 5. Images of fluorescent beads (140 nm diameter) in different steps during the reconstruction process. The real space images are always shown to the left. The logarithm of the magnitude square of the fourier transform (+1) of the image to the left is always shown to the right. The zero frequency is displayed in the centre of the right images. White arrows indicate the positions of the peaks with zero object frequency. *(a,b):* A measured image and its fourier transform; *(c,d):* subtraction of two 180° phased images. *(e,f):* Subtraction of the 90° and the 270° image.

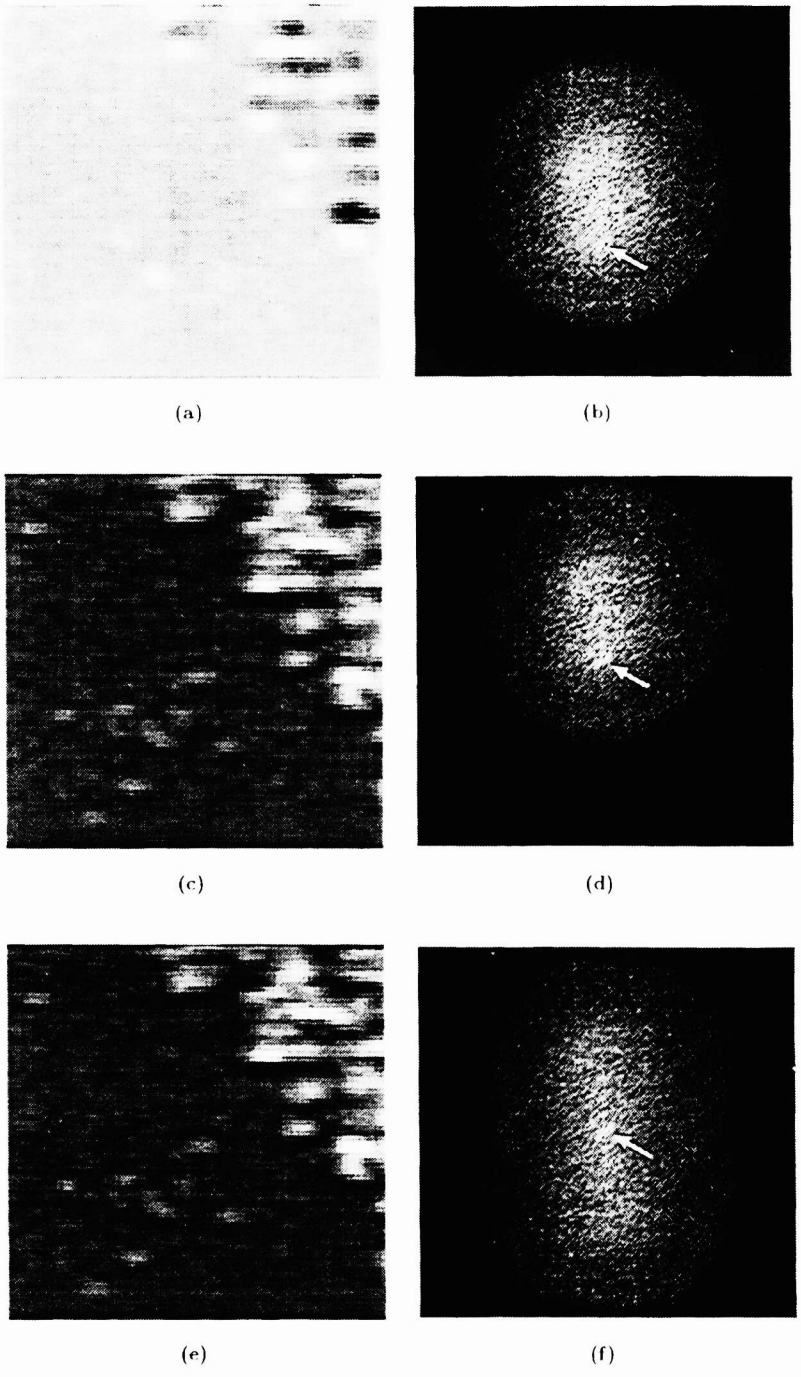

Figure 6. Further Steps of the reconstruction process: *(a,b):* Figure 5(e) was multiplied with i and subtracted from Figure 5(c). In this way one illumination component could be extracted. Only the uninfluenced real part is shown in (a). *(c,d):* By multiplying the real-space image (a) with $\exp(ikx + \varphi)$, the sideband was shifted to the central position. φ was chosen such that the zero frequency component was real. Only the real part of the image is shown in (c). *(e,f):* Adding the complex-conjugate in real-space resulted into a self-adjoint fourier transform.

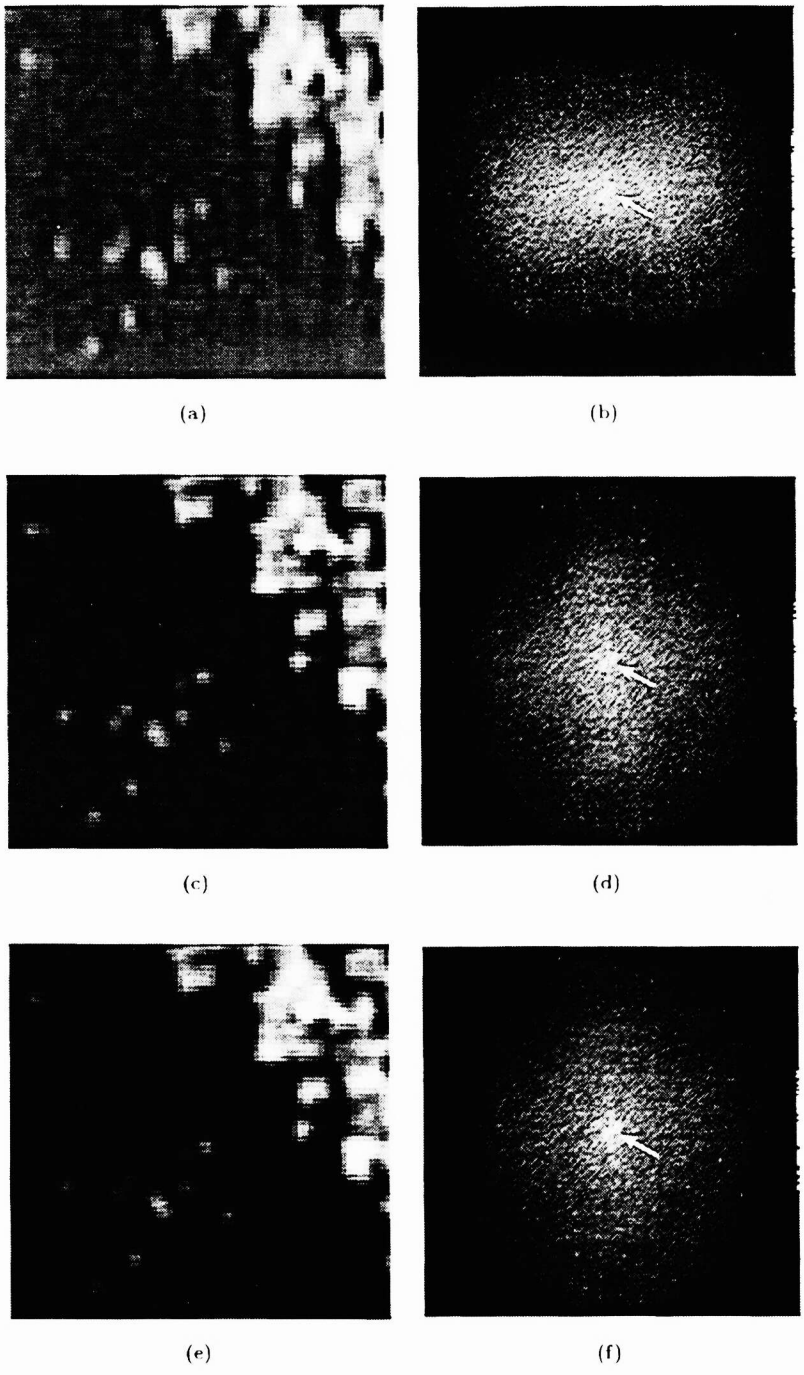

Figure 7. Continuation of the reconstruction process: *(a,b):* The same procedure as in Figure 5 and 6 was applied to the images obtained with the diffraction grating rotated by 90° *(c,d):* Addition of the two reconstructed datastacks for perpendicular diffraction gratings. *(e,f):* The sum of the eight original datastacks for all eight illumination phases was added to the central image with a weight of 1/26, to enhance the suppressed low frequencies.

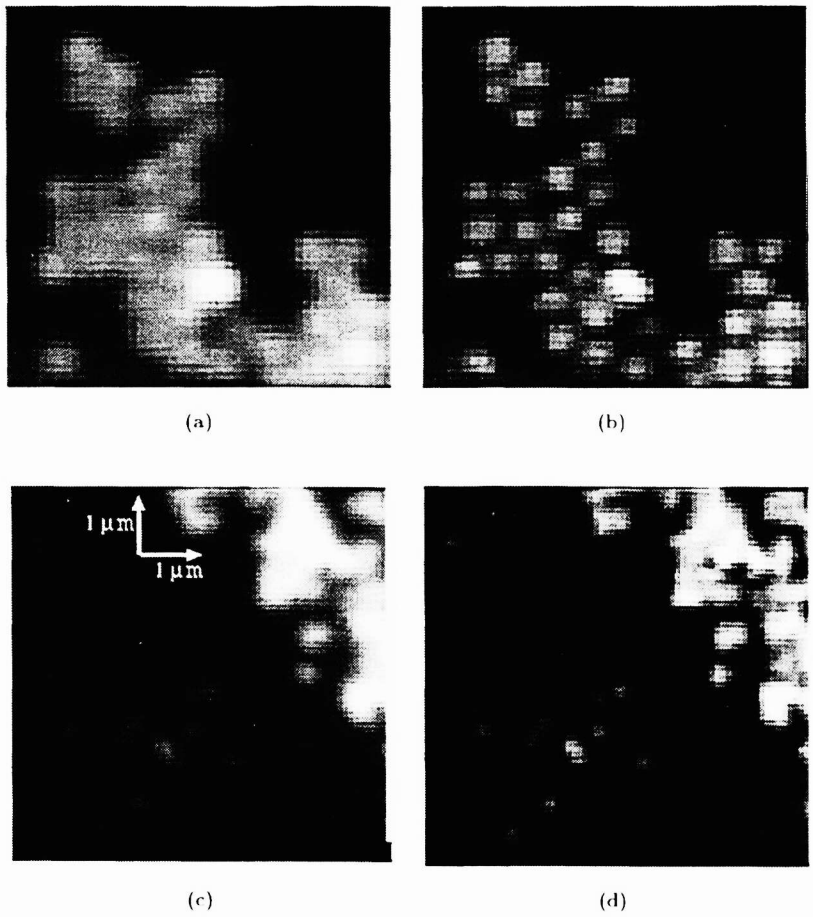

Figure 8. *(a):* A cluster of microscopical quartz beads (416 nm in diameter with a 200 nm fluorescent RITC core) imaged by the method of laterally modulated excitation microscopy. This image was obtained, after the data from the four different phases were back shifted and added. Its resolution is expected to be the resolution of a conventional epifluorescent microscope. *(b):* Image of the same dataset as in (a) reconstructed using the LMEM reconstruction algorithm described above. *(c) and (d):* Analogous comparison for 140 nm micro beads shown during the reconstruction process in Figures 5 to 7.

A comparison of the image qualities obtained is shown in Figure 8. Visually a clear improvement of the images by using the LMEM reconstruction algorithm is apparent. The image 8(d) can also be compared to image 5(a). In Figure 9 quantitative intensity line scans suggest that the reconstruction process indeed increased the discrimination of partially "overlapping" images of small particles (beads with a diameter of 416 nm). The lateral FWHM of a single bead with a nominal diameter of 140 nm was found to be about 330 nm for the image obtained by adding all phases and 230 nm for the presented LMEM reconstruction method. This was determined by evaluating the intensities of three single beads shifted such, that their centre of intensity was aligned (see Figure 9(d)).

A threshold based segmentation was applied to image (b) in Figure 8 resulting into 31 clearly distinguished objects using a threshhold of 30% of the maximum intensity in the image. The mean distance from the centre of intensity of one object to the nearest neighbouring object centre of intensity was found to be 402 nm. The standart deviation of the histogram of nearest neighbour distances was 90 nm. The value of 402 nm is in good agreement with the nominal distance of 416 nm of two attached beads. Without using the presented reconstruction algorithm (Figure 8(a)) it was not possible to discriminate a significant number of individual beads using any global threshhold value.

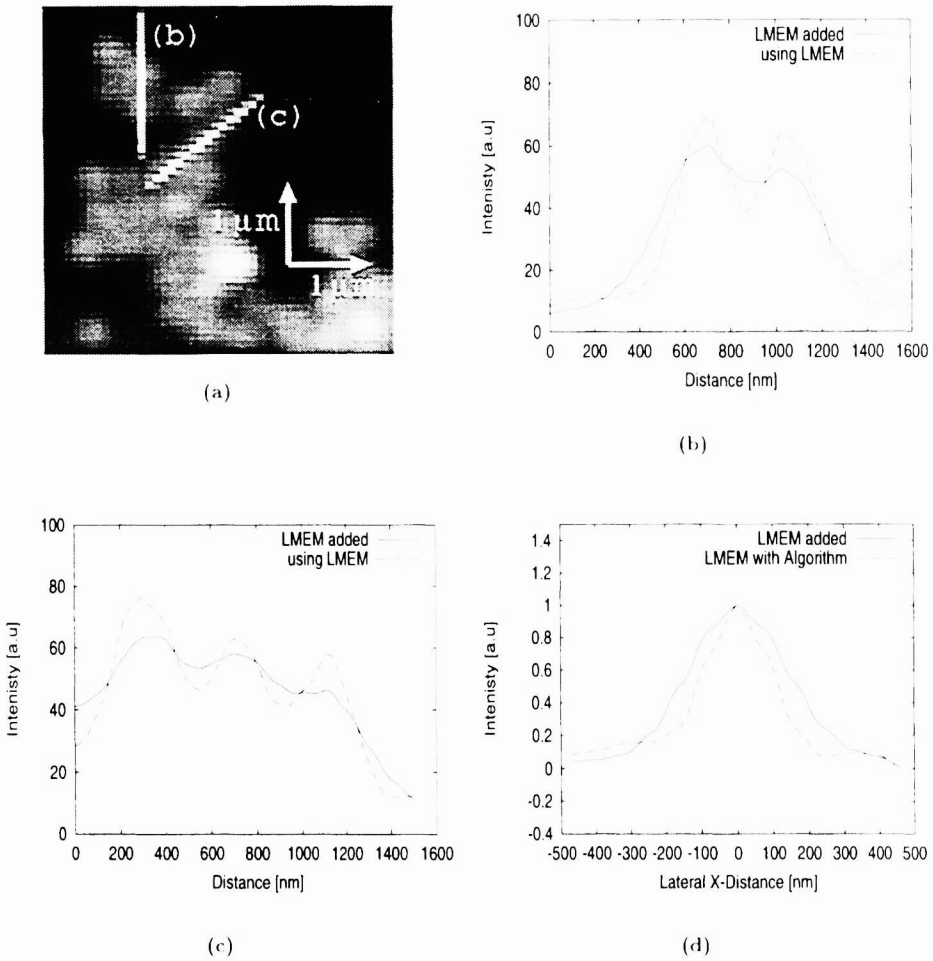

Figure 9. Intensity line scans through RITC quartz beads (416 nm diameter) shown in Figure 8(a,b) being attached to each other. The intensity line scan of the added back shifted images (equivalent to a normal microscopic image) is shown in comparison with a line scan through an image obtained using LMEM with the described algorithm (a): Lines in the image (see Fig. 8(a) and 8(b) respectively) indicate where the intensity of (b) and (c) was evaluated. *(d):* Intensity line scan comparison through an overlay image of three beads (140 nm diameter).

5. DISCUSSION

The method of lateral modulated excitation microscopy (LMEM) combined with a suitable reconstruction algorithm seems to be a useful way to improve the lateral resolution of the epifluorescence microscope in a way that is easy to implement into conventional microscopes. The method is based on an enlargement of the principally detectable object spatial frequencies and thus is qualitatively different from deconvolution methods such as Wiener filtering or maximum likelihood (ML) deconvolution. Data acquisition and evaluation could be further expanded to the 3D case to make use of the possibility of optical sectioning (see T. Wilson et al.[2]).

A different diffraction grating producing the four necessary diffraction orders in two dimensions simultaneously would make it possible to eliminate the step of rotating the grating relative to the object. With a motorised movable grating, a fast online reconstruction should be possible, since the computational effort for reconstruction is small. An appropriate arrangement of split laser beams could be phase-shifted by phase shifting their individual beams in relation to the others. The method may be combined with other image restoration methods as for example maximum likelyhood reconstruction for further improvement of resolution by deconvolution. Using ML deconvolution

on normal microscopic images and comparing the results to ML deconvoluted images using LMEM is planned for future investigation.

Suppression of the zero order together with a light source of high luminosity and a more sophisticated binary coded grating may increase the modulation depth and therefore the efficiency. The same may be achieved by illuminating with a split laser beam through the objective lens. If a mounting is constructed that makes it possible to illuminate the object with a split laser beam directly one would not be restricted to the numerical aperture of the objective lens in the illumination pathway, and the total resolution of the system might be improved beyond the factor of two.

As described by Gustafson,[5] resolution improvement can be achieved by a mutual coherent illumination and detection of as many spatial frequencies as possible. This is the basic principle that was used for lateral modulated excitation microscopy. It is also used extensively in I^5M-microscopy[6] and 4-pi-microscopy.[7]

In standing wave field microscopy[8] and spatially modulated excitation microscopy[9] a very high spatial illumination frequency is normally used in axial direction. That is a similar principle as LMEM, only the direction of modulation is different. This results, however, in a part of spatial frequencies missing in the overall detection, making it impossible to reconstruct high resolution images from the measured data without further assumptions about the object structure. If such approaches were combined with LMEM by illuminating from two sides into 4 directions, a very high overall 3D resolution should be obtainable.

So far, only a slight resolution improvement of about 40% was achieved, as judged from a comparison of the experimentally obtained FWHM. Further studies using a grating with improved modulation depth and smaller fringe distance or a split laser beam illumination are required to optimise the LMEM method.

6. ACKNOWLEDGEMENTS

We greatfully acknowledge the support of the "Graduiertenkolleg Tumordiagnostik und -Therapie unter Einsatz dreidimensionaler radiologischer und lasermedizinischer Verfahren", of the Deutsche Forschungsgemeinschaft.

Many thanks also to the "Sensorik und Mikrostrukturen" group of the Institute of Applied Physics, University of Heidelberg, for manufacturing the diffraction grating with photo-lithographic techniques.

REFERENCES

1. S. Inoue, "Foundations of confocal scanned imaging in light microscopy," in *Handbook of Biological Confocal Microscopy*, J. B. Pawley, ed., ch. 1, Plenum Press, New York, second ed., 1995.
2. T. Wilson, R. Juskaitis, and M. Neil, "A new approach to three dimensional imaging in microscopy," *Cell Vision* **4**, p. 231, March / April 1997.
3. R. Windecker, M. Fleischer, and H. Tiziani, "Three-dimensional topometry with stereo microscopes," *Optical Engeneering* **36**, pp. 3372–3377, December 1997.
4. N. A. M. Verhaegh and A. von Blaaderen, "Dispersion of rhodamine-labeled silica spheres: Synthesis, characterization, and fluorescence confocal scanning laser microscopy," *Langmuir* **10**, pp. 1427–1438, 1994.
5. D. A. M. Gustafson and J. Sedat, "Sevenfold improvement of axial resolution in 3d widefield microscopy using two objective lenses," *Proceedings of the SPIE* **2412**, pp. 147–156, 1995.
6. D. A. M. Gustafson and J. Sedat, "3d widefield microscopy with two objective lenses: Experimental verification of improved axial resolution," *Proceedings of the SPIE* **2655**, p. 62, 1996.
7. S. Lindek, E. Stelzer, and S. Hell, "Two new high-resolution confocal fluorescence microscopies (4pi, theta) with one- and two-photon exitation," in *Handbook of Biological Confocal Microscopy*, J. B. Pawley, ed., ch. 26, pp. 417–429, Plenum Press, New York, second ed., 1995.
8. F. Lanni, B. Bailey, D. Farkas, and D. Taylor, "Excitation field synthesis as a means for obtaining enhanced axial resolution in fluorescence microscopes," *Bioimaging* **1**, pp. 187–196, 1993.
9. B. Schneider, J. Bradl, I. Kirsten, M. Hausmann, and C. Cremer, "High precision localization of fluorescent taargets in the nanometer range by spatially modulated excitation microscopy," *Fluorescence Microscopy and Fluorescent Probes* **2**, pp. 71–76, 1997.